Chemical Engineering Journal 164 (2010) 77–84

Contents lists available at ScienceDirect

Chemical Engineering Journal

journal homepage: www.elsevier.com/locate/cej

Effects of synthesis conditions and annealing post-treatment on the photocatalytic activities of ZnO nanoparticles in the degradation of methylene blue dye

Okorn Mekasuwandumrong[a], Pongsapak Pawinrat[b], Piyasan Praserthdam[b], Joongjai Panpranot[b,*]

[a] Department of Chemical Engineering, Faculty of Engineering and Industrial Technology, Silpakorn University, Nakorn Phathom 73000, Thailand
[b] Center of Excellence on Catalysis and Catalytic Reaction Engineering, Department of Chemical Engineering, Faculty of Engineering, Chulalongkorn University, Bangkok 10330, Thailand

ARTICLE INFO

Article history:
Received 8 March 2010
Received in revised form 11 August 2010
Accepted 11 August 2010

Keywords:
Flame-spray pyrolysis
ZnO
Particle size effect
Photocatalysts
Annealing

ABSTRACT

The effects of synthesis conditions (i.e., metal concentration, precursor flowrate, and O_2 dispersion) during flame-spray pyrolysis (FSP) and annealing post-treatment on the characteristics and photocatalytic activities of ZnO nanoparticles have been investigated. The average particle size of ZnO powder prepared by one-step FSP method were in the range of 8.8–47.0 nm and were found to be increased with increasing the enthalpy density, flame height, and high-temperature residence time during FSP synthesis. The larger particle size FSP-derived ZnO nanoparticles exhibited higher photocatalytic activities in the degradation of methylene blue (MB) dye. The degradation rate over FSP-ZnO-47.0 nm was 1.7 and 7.2 times higher than those of the commercially available photocatalysts Degussa P-25 and JRC-TiO_2, respectively. The better photocatalytic performance of the FSP-ZnO was correlated well with the improved crystalline quality of ZnO nanoparticles as revealed by the X-ray diffraction (XRD) and the photoluminescence (PL) results. Further increase of FSP-ZnO particle size to 52.6–103.5 nm by annealing post-treatment at high temperatures (750–900 °C), however, gradually decreased their photocatalytic activities. Our results in this study suggest a balance between high crystalline quality that enhanced photo phenomena and the surface area available for substrate adsorption in order to obtain high photocatalytic activity of ZnO nanoparticles.

1. Introduction

Dye pollutants from textile paper and other industries are an important source of environmental contamination. Conventional treatment of such wastewater generally involves coagulation/flocculation [1,2], electrocoagulation [3], coagulation/carbon adsorption process [4] and so on. These methods, however, merely transfer dyes from the liquid-phase to the solid-phase, requiring further treatment and causing secondary pollution [5]. In the past two decades, photocatalysis by semiconductive materials such as TiO_2 and ZnO has attracted public concern as a promising tool among the advanced oxidation processes to substitute the traditional wastewater treatment due to their high photosensitivity, non-toxic nature, high stability, and wide band gap [6]. While TiO_2 is probably the most frequently used photocatalyst, ZnO is an alternative photocatalyst with low cost. It has a similar band gap energy compared to TiO_2 (3.2 eV) [7] and can adsorb over a larger fraction of UV spectrum [8]. Higher photocatalytic efficiency of ZnO compared to TiO_2 has been reported especially for degradation of organics in aqueous solutions [5,9–13]. Our recent study showed that Au–ZnO and Pt–ZnO nanocomposites prepared by one-step flame-spray pyrolysis exhibited high photocatalytic activities in degradation of methylene blue dye [14].

For semiconductor photocatalysts, particle size is an important parameter for controlling surface area and electronic structure. When the catalyst particle size is reduced down to a few nanometers, an elevate density of active sites for substrate adsorption and/or catalysis can be guaranteed, as small particles possess a significantly higher surface-to-volume ratio compared to the bulk material. When the nanocrystal size is comparable or smaller than the bulk exciton diameter, the band-gap becomes size-dependent due to quantization effects [15,16]. Moreover, an efficient photocatalytic process requires highly crystalline semiconductors to minimize electron–hole pair loss owing to the trapping of either charge carriers at defect states [17,18].

The effect of particle size on photoactivity of ZnO has been addressed by a number of researchers [19–22]. For examples, among the three different particle sizes of ZnO nanoparticles (14,

* Corresponding author. Tel.: +66 2218 6869; fax: +66 2218 6877.
E-mail address: joongjai.p@chula.ac.th (J. Panpranot).

1385-8947/$ – see front matter © 2010 Elsevier B.V. All rights reserved.
doi:10.1016/j.cej.2010.08.027

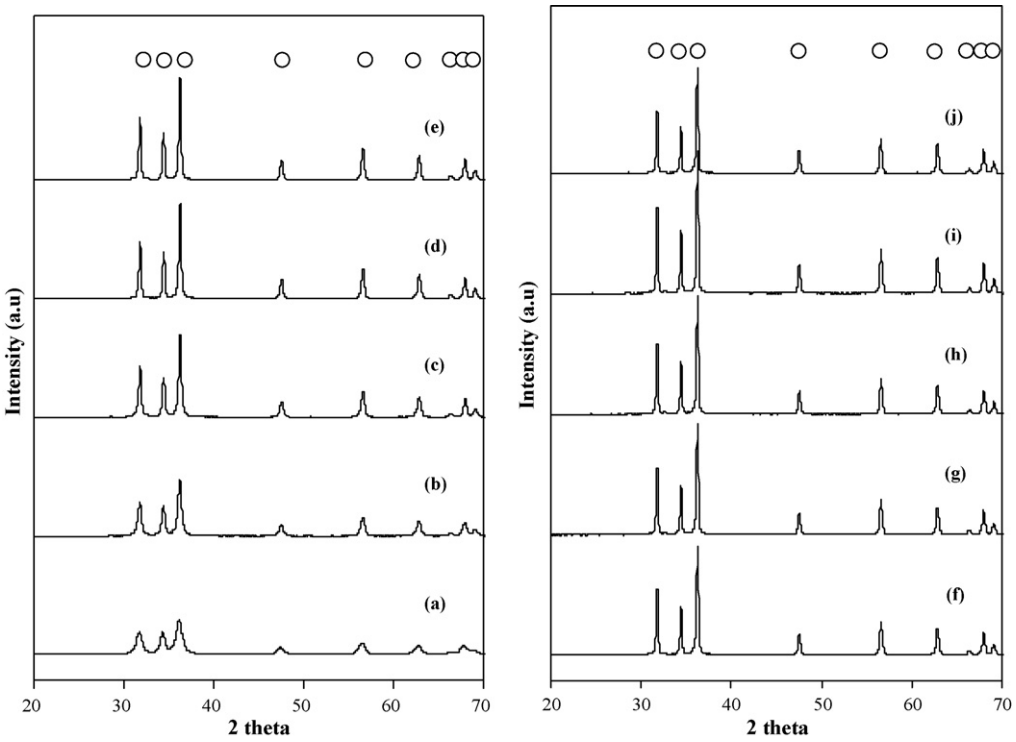

Fig. 1. XRD patterns of the as-prepared flame-made ZnO with various crystallite sizes: (a) 8.8 nm, (b) 19.4 nm, (c) 30 nm, (d) 40.7 nm, (e) 47 nm and the annealed flame-made ZnO particles: (f) 52.6 nm, (g) 67.1 nm, (h) 80.3 nm, (i) 90.6 nm, (j) 103.5 nm.

19, and 26 nm) prepared by precipitation process, the smaller one resulted in more surface oxygen vacancies, higher ESR intensity, stronger PL signal, and higher photocatalytic activity [20]. Dodd et al. [21] prepared ZnO nanoparticles with various particle sizes in the range of 28–57 nm by mechanical milling and heat treatment. The authors found that there exists an optimum size of 33 nm for which the photocatalytic activity of ZnO is maximized. Li et al. [22] also obtained ZnO nanoparticles with average sizes 21–90 nm by varying the calcination temperature between 200 and 1000 °C and found that ZnO prismatic aggregated obtained by calcination at 800 °C demonstrated the highest photocatalytic activity. More recently, Xie et al. [19] showed that photocatalytic properties of various particle sizes of ZnO (15, 50, 200, and 1000 nm) synthesized by thermal evaporation and chemical deposition in UV-induced degradation of methyl orange depended on size, morphology, and preparation method of ZnO. Thus, in previous studies, it has clearly shown that efficiency of photocatalytic process can be maximized by optimizing the particle size of ZnO photocatalysts. However, preparation method as well as pretreatment conditions such as calcination temperature strongly affects the properties of ZnO photocatalysts.

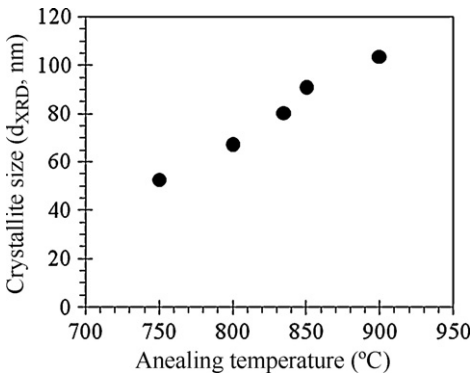

Fig. 2. Relationship between crystallite size of ZnO and annealing temperature.

In this report, ZnO nanoparticles with various particle sizes were obtained by flame-spray pyrolysis (FSP) method. Various particle sizes of the flame-made ZnO powder (8.8–103.5 nm) were obtained by varying the process conditions such as metal concentration in

Table 1
Relationship between the synthesis conditions and ZnO crystallite sizes.

Metal concentration (molar)	Precursor flow rate (ml/min)	Dispersion oxygen flow rate (l/min)	Annealing temperature (°C)	Crystallite size d_{XRD} (nm)	Average primary particle size d_{TEM} (nm)	BET surface area (m^2/g)
0.3	3	5	n/a	8.8	11.1	63.1
0.3	8	3	n/a	19.4	20.5	35.5
0.5	8	3	n/a	30.0	31.3	26.2
0.8	8	3	n/a	40.7	39.8	13.6
1	8	3	n/a	47.0	48.7	15.1
1	8	3	750	52.6	57.7	12.0
1	8	3	800	67.1	71.7	8.0
1	8	3	835	80.3	98.9	6.8
1	8	3	850	90.6	116.7	5.9
1	8	3	900	103.5	159.9	5.8

n/a = not applied.

feed, precursor flow rate, dispersion oxygen flow rate, and annealing temperature. The effects of both FSP synthesis conditions and annealing post-treatment on the characteristics and photocatalytic properties of the flame-made ZnO in photodegradation of methylene blue (MB) were discussed extensively.

2. Material and methods

2.1. Synthesis of ZnO nanoparticles by flame-spray pyrolysis

Synthesis of ZnO with various particle sizes by FSP technique were carried out using a spray flame reactor [24]. Zinc naphthanate (Aldrich; <50% in mineral spirits) was used as zinc precursor. The precursor was dissolved in ethanol (J.T. Baker; 99.9%). To obtain different ZnO particle sizes during particle synthesis, precursor solution ranged from 0.3 to 1 mol/l and liquid precursor feed rates varied from 3 to 8 ml/min were fed to the flame by a syringe pump. Precursors were dispersed with 3–5 l/min oxygen forming fine spray droplets. The pressure drop at the capillary tip was maintained at 1.5 bar by adjusting the orifice gap area at the nozzle. The reactor was water-cooled to avoid evaporation or decomposition of the precursor within the feed lines. The flame was ignited by a concentric premixed methane/oxygen pilot flame (CH_4 1.5 l/min, O_2 3.0 l/min) that was sheathed further by flowing oxygen (25 l/min) through a sintered metal plate ring (8 mm wide,

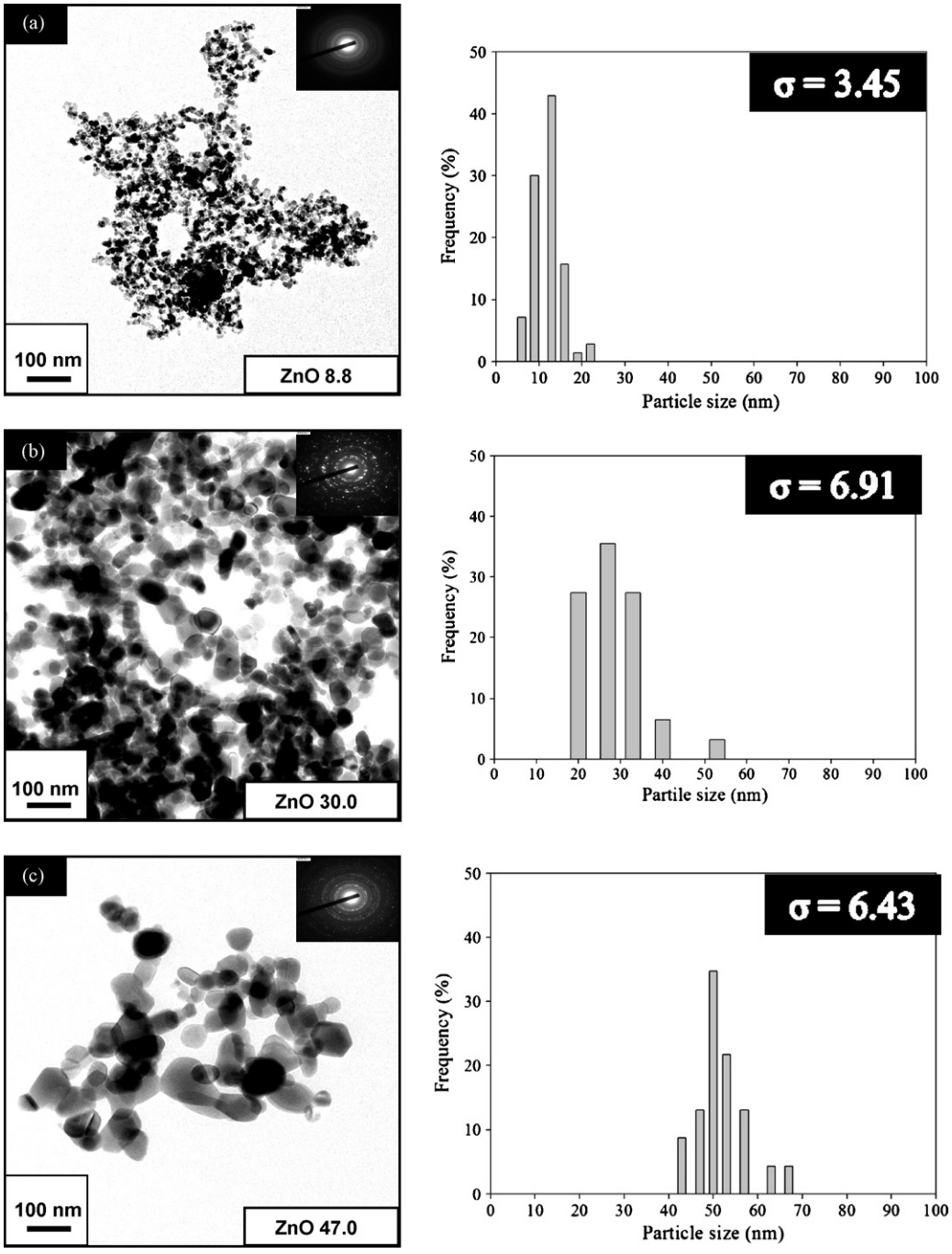

Fig. 3. TEM micrographs, SAED patterns, and particle size distribution of the as-synthesized FSP-made ZnO particles: (a) 8.8 nm, (b) ZnO 30.0 nm, (c) ZnO 47.0 nm and the annealed ZnO: (d) 67.1 nm, (e) 80.3 nm, (f) 103.5 nm.

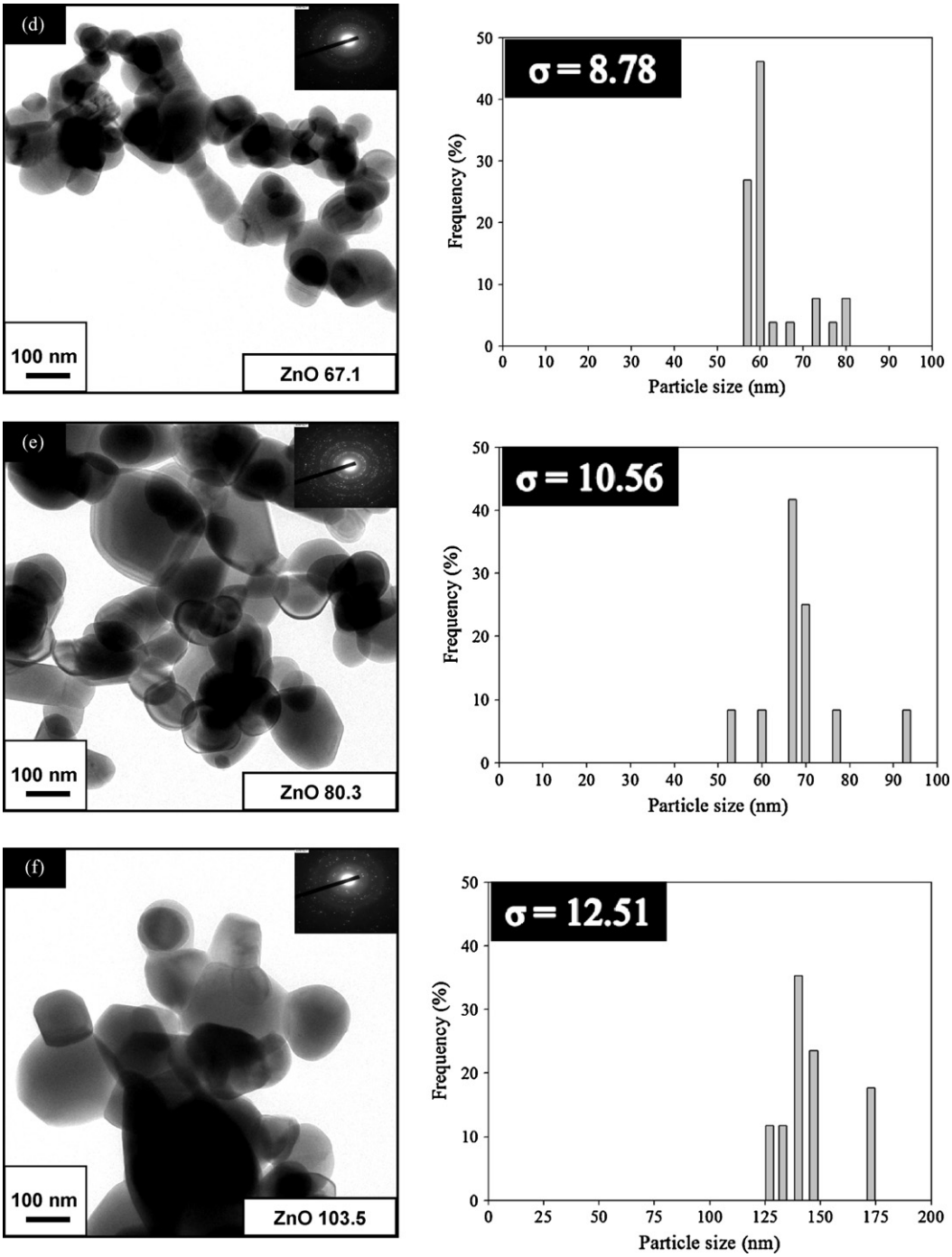

Fig. 3. (*Continued*)

starting at a radius of 8 mm). The powder particles were collected on a glass–fiber filter (GF/D Whatman; 257 mm diameter) with the aid of a vacuum pump.

2.2. Annealing of the flame-made ZnO

Annealing of the ZnO powders was performed in a Carbolite CWF1300 temperature programmed box furnace in static air, ZnO powders with the particle size of 47 nm produced by FSP method were heated at 10 °C/min to desired temperature (750, 800, 835, 850, or 900 °C) and maintained at that temperature for 1 h in order to form larger particles.

2.3. Characterization

Powder X-ray diffraction (XRD) was performed by a SIEMENS XRD D5000 diffractometer using Cu Kα radiation. The crystallite size (d_{XRD}) of FSP-ZnO powders was estimated from the full-width half-maximum breadth of the (1 0 1) diffraction peak using the Scherrer equation. The specific surface area was measured by N_2 physisorption using a Micromeritics ASAP 2000 automated system and the Brunauer–Emmet–Teller (BET) method. Each sample was degassed under vacuum at $<1 \times 10^{-5}$ bar in the Micromeritics system at 300 °C for 3 h prior to N_2 physisorption. The particle morphology was observed using JEOL Model JEM-

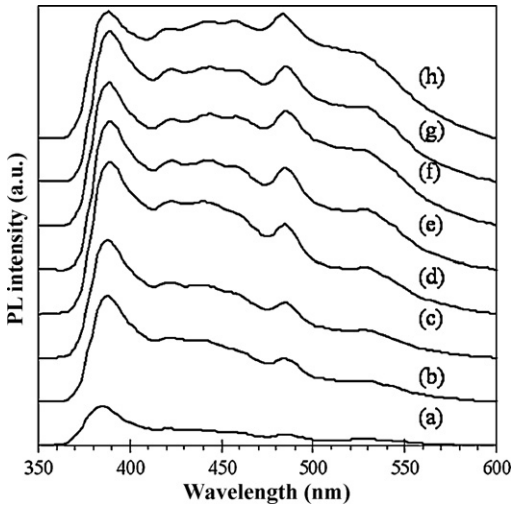

Fig. 4. PL spectra of various ZnO particle sizes prepared by FSP method (a) ZnO 8.8 nm, (b) ZnO 19.4 nm, (c) ZnO 30.0 nm, (d) ZnO 47.0 nm, (e) ZnO 67.1 nm, (f) ZnO 80.3 nm, (g) ZnO 90.6 nm, and (h) ZnO 103.5 nm with the excitation wavelength of 325 nm.

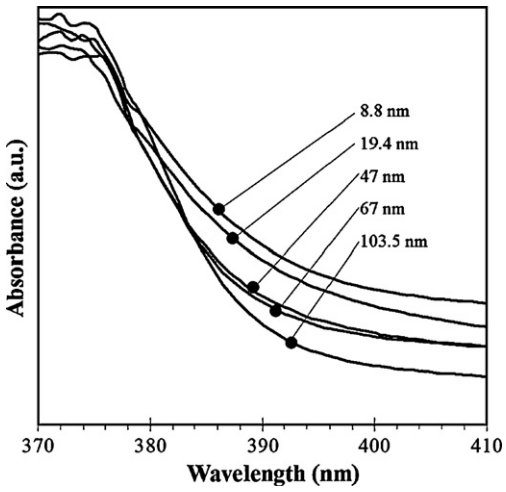

Fig. 5. UV–vis spectra of ZnO with various particle sizes.

2010 transmission electron microscope (TEM) operated at 200 keV. Photoluminescence measurement (PL) was carried out on a fluorescence spectrophotometer (Perkin-Elmer LS-50) using a Xenon lamp as the excitation source at room temperature. The sample was dispersed in ethanol using ultrasonic bath and the excitation wavelength used in PL measurement was 325 nm.

2.4. Photocatalytic activity testing

A basic aniline dye, methylene blue (MB), from Unilab Asia Pacific Specialty Chemicals Limited was used as a probe molecule to evaluate the photocatalytic activities of the flame-made ZnO with various particle sizes. The photocatalytic reaction was conducted at room temperature under UV light 2×15 W UV tube predominantly emitting at 365 nm (Philips) with the average light intensity on the reaction beaker (pyrex) at a distance of 6 cm from the lamp was found to be 4.7×10^{-4} W cm^{-2}. The reaction was carried out with 20 mg of catalyst dispersed in 200 ml of 10 ppm methylene blue aqueous solution. The pH of solution was constant at 6.3 for all experiments. The reaction was operated with high stirring rate (1000 rpm) in order to eliminate the external mass transfer effect. Prior to irradiation, the suspensions were magnetically stirred in the dark for 15 min to establish the adsorption/desorption equilibrium of methylene blue. 2 ml samples were withdrawn every 10 min. Before analysis, the aqueous samples were centrifuged to remove any suspended solid catalyst particles. The residual concentration of methylene blue was measured at 665 nm using the UV–vis spectrophotometer (Perkin-Elmer lampda 650) in liquid cuvette configuration with de-ionized water as reference. The percentage of degradation was calculated using the equation given below:

$$\text{Degradation}\ (\%) = \frac{C_0 - C}{C_0} \times 100 \quad (1)$$

in which C_0 is the initial dye concentration and C is the dye concentration after the treatments.

3. Results and discussion

3.1. Particles characterization

Fig. 1a–e shows the XRD patterns of as-synthesized FSP-ZnO nanopowder with average crystallite sizes between 8.8 and 47.0 nm. All of the indexed peaks are well matched with that of bulk ZnO (JCPDS Card No. 36-1451) possessing wurtzite hexagonal phase. No other diffraction peaks or amorphous phase was detected. The diffraction peak intensities were increased and the peaks became sharper with increasing ZnO particle sizes. The larger particle sizes of ZnO particles were obtained by increasing the precursor concentration, the ratio of the feed liquid, and decreasing the dispersion oxygen gas flow rates through the nozzle. Fig. 1f–j shows the XRD patterns of the annealed ZnO powders. The XRD characteristic peaks were similar to those of the as-synthesized ones. The calculated particle sizes of annealed ZnO were in the range of 52.6–103.5 nm indicating that annealing of the flame-made ZnO particles (47 nm) at relatively high temperature between 750 and 900 °C resulted in further crystal growth of ZnO. The relationship between synthesis conditions and corresponding ZnO particle sizes are summarized and illustrated in Table 1 and Fig. 2, respectively.

The TEM micrographs with selected area electron diffraction (SAED) patterns and particle size distribution of the as-synthesized and the annealed ZnO with various particle sizes are shown in Fig. 3. Frequency (%) was obtained by counting 50–100 ZnO particles from TEM images. All the samples consisted of polyhedral primary particles, typically seen in flame-made powders [23], with spheroidal particles and rod-like particles. The average primary particle diameters of ZnO with various particle sizes determined by TEM (d_{TEM}) are also given in Table 1. The d_{TEM} data were in good agreement with the d_{XRD} values. The corresponding SAED patterns are shown in the

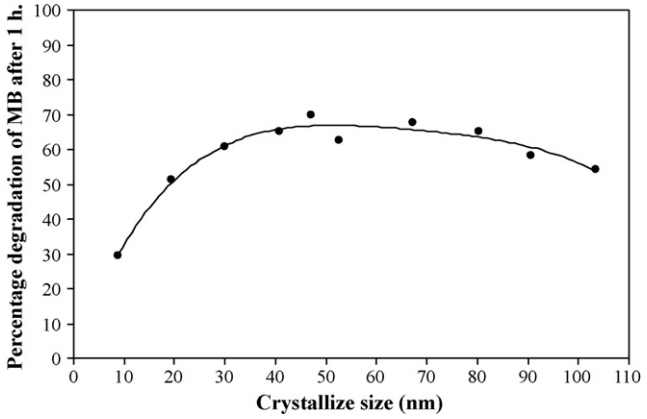

Fig. 6. Relationship between for the percentage of MB degradation after 1 h and the particle size of ZnO photocatalysts prepared by FSP method.

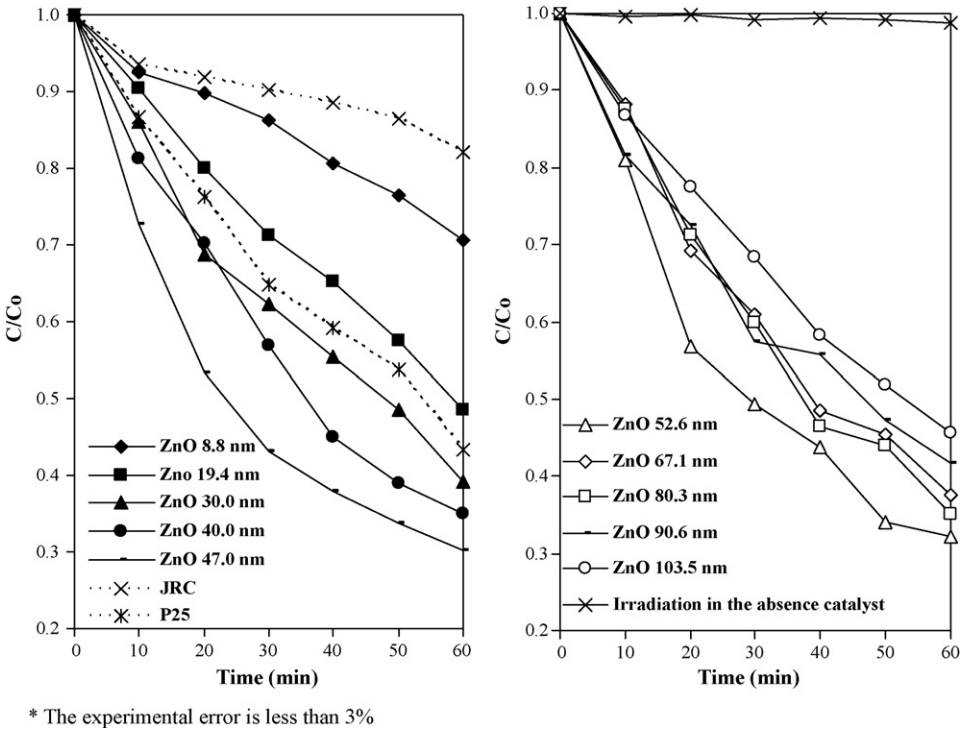

Fig. 7. The catalytic performances for photodegradation of methylene blue using FSP-made ZnO catalysts with various particle sizes (bold lines) and commercial catalysts for comparison (P25 and JRC titania) (dashed lines).

insets. The diffraction patterns of all the powders illustrate spot patterns of the hexagonal structure of ZnO, indicating that the ZnO nanoparticles are single crystalline. As also shown in Table 1, BET surface areas of the as-synthesized ZnO particles decreased from 63.1 to 15.1 m^2/g as the precursor concentration increased from 0.3 to 1 M and the feed rate increased from 3 to 8 ml/min. The result was consistent with previous studies of the flame-synthesized metal oxides such as TiO_2 [25], SiO_2 [26], CeO_2 [27], Pt/Al_2O_3 [28], and Ag/ZnO [29]. Typically, increasing of precursor feed flow rate and/or precursor concentration while keeping the oxygen flow rate constant results in higher enthalpy of flame, longer residence times and hotter flames [24,25]. This phenomenon is due to the fact that the combustion of the precursor is an exothermic reaction, contributing to overall increase in energy dissipation within the flame. Additionally, as the precursor feed flow rate and precursor concentration increased, Zn concentration within the flame also increased. This, coupled with the increased enthalpy content, residence time and higher flame temperature, resulted in increased coalescence and sintering of the particles. After high-temperature annealing (750–900 °C), the BET surface areas decreased further from 15.1 to 5.8 m^2/g indicating that ZnO particles sintered by heat treatment.

Room temperature PL spectra of all the ZnO powders are shown in Fig. 4. The spectra mainly consisted of two emission bands. The first band is the UV near-band-edge emission (NBE) at ~385 nm [30,31]. Sharp NBE emission peak results from recombination of excitons and its position and structure is an indication of crystal quality [32,33]. The NBE emission intensities in the PL spectra increased as the particle size of as-synthesized ZnO increased. The highest value was found for the FSP-made ZnO with the crystallite size of 47 nm. Improvement of the crystal quality of ZnO can be attributed to the increase of flame enthalpy and Zn atomic concentration in gas phase that contributed typically to longer and hotter flames, which as a consequence, produced larger and more crystalline particles. However, the excitonic peak intensity for the annealed samples was remained constant and slightly decreased as the annealing temperature was raised higher than 835 °C. Moreover, the shift to the lower wavelength was also found in the FSP-made ZnO with the crystallite size of 8.8 nm. This result would be attributed to the quantum confinement effect of ZnO nanoparticles [34,35]. Madler et al. [35] prepared the ZnO quantum dots by spray combustion of Zn/Si precursors. These crystallites exhibit a quantum size effect due to the preventing of the growth and stabilized the ZnO crystals. The blue shift of the ultraviolet–vis absorption edge increased with decreasing ZnO crystal size. The other band observed in PL spectra was the visible emission that usually associates with the deep level emission (DLE) in ZnO. Most researchers believe that the DLE come from oxygen vacancies (V_O), zinc vacancies (Zn_O), interstitial zinc (Zn_i), or interstitial oxygen (O_i) [36,37]. The blue emission at ~425 nm and weak blue at ~445 nm most likely occurs from the donor level of Zn interstitial (Zn_i) to acceptor energy level of Zn vacancy (Zn_O) [38]. The blue–green band around 470 nm was probably caused by radiative

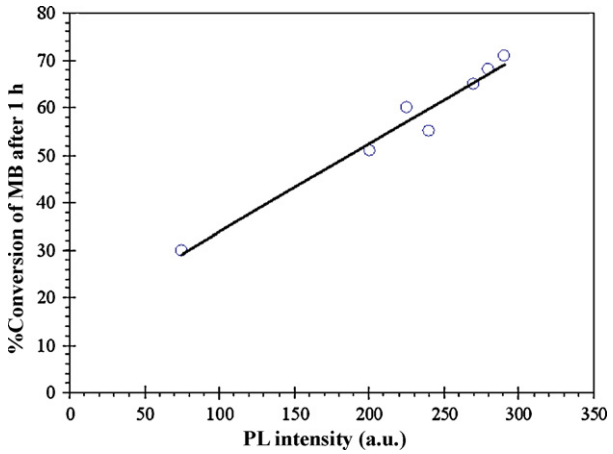

Fig. 8. Relationship between percentage of conversion of MB after 1 h of UV irradiation and PL intensity of the ZnO particles.

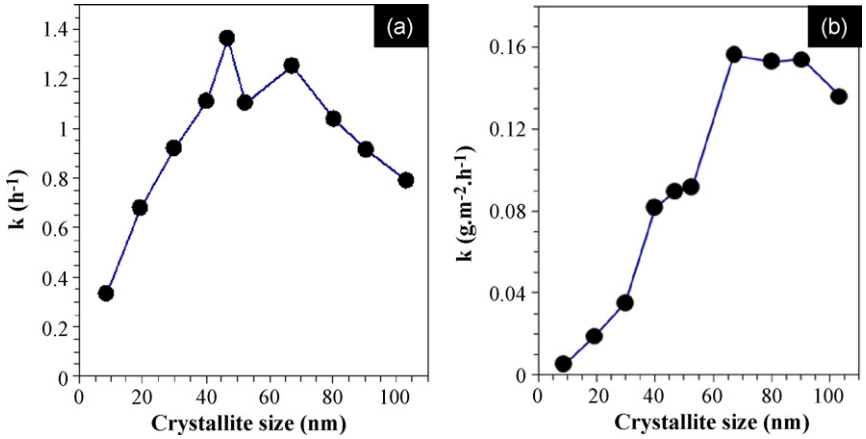

Fig. 9. Pseudo first-order rate constants for ZnO catalysts with various crystallite sizes on a mass (a) and SSA normalized (b) basis.

transition of electron from shallow donor levels, created by the oxygen vacancy to valence band [39]. The green emission at ~530 is commonly observed for ZnO, and was attributed to the singly ionized oxygen vacancy in ZnO [40]. This emission results from the recombination of a photo-generated hole with the singly ionized charge state of the specific defect [41]. The peak intensity of the blue and weak blue peak light emission increased with increasing of ZnO crystallite size from 8.8 to 47.0 nm and then was found remained unchanged. The weak blue–green band and green band emission peaks intensity slightly increased with increasing crystallite size from 8.8 to 103.5 nm.

Fig. 5 shows UV–vis absorbance spectra of the FSP-made ZnO powders. It can be seen that the slope of UV–vis spectra of the FSP-made ZnO powder was steeper from the smallest size of 8.8 nm to the size of 47 nm before reaching a plateau. A sharp UV–vis absorption curve (steep slope) indicates a high degree of crystalline quality [29]. The improved crystal structure for the larger size ZnO was in good agreement with the XRD and PL-measurements.

3.2. Photocatalytic activity

The dependence of percent conversion of MB decomposition after 60 min on the particle size of ZnO powders is shown in Fig. 6. Irradiation in the absence of photocatalyst for 60 min revealed no change in the MB concentration, confirming that the MB cannot be degraded by 365 nm irradiation alone. The percentages of MB degradation increased from 30 to 70% when the particle size of as-synthesized ZnO powders increased from 8.8 to 47 nm. The photocatalytic performances for MB degradation of the as-synthesized and annealed FSP-ZnO catalysts are also shown as the plots of (C/C_0) versus time in Fig. 7 in which the results for commercial photocatalysts *Degussa* P25 (d_{XRD} = 20.1 nm) and JRC-TiO-1 titania (d_{XRD} = 15.5 nm) and irradiation in the absence of catalyst are included. The photocatalytic activity of the as-synthesized flame-made ZnO powders was superior to both P25 and JRC-TiO-1 titania when their particle sizes were larger than 30 nm with the as-syn ZnO-47 nm showed the highest activity. The rate constant assuming first-order kinetics of ZnO-47 nm was determined to be 1.7 and 7.2 times higher than those of degussa P25 and JRC-TiO-1 titania, respectively. For the larger particle sizes of ZnO powder obtained by annealing post-treatment, the percentages of MB degradation gradually decreased from 70 to 55%. The lower photocatalytic efficiency can be ascribed by the decrease in BET surface area, which lowered the adsorption of dye molecules on the catalyst surface.

In general, photocatalysis can be considered to be dominated by two linked mechanisms, namely photo phenomena or the interaction of light with the material to form electron–hole pairs, and secondly surface catalytic effects [42]. The photo aspect is sensitive to crystal defects while the surface catalytic effect is mainly dominated by the specific surface area. In this study, the photocatalytic performance of FSP-ZnO nanoparticles was found to increase with increasing crystalline quality of ZnO as illustrated by a linear relationship between the PL intensity of NBE bands and the percent conversion of MB decomposition after 60 min (Fig. 8). It is suggested that the photo phenomena (the interaction of light with the material to form electron–hole pairs) played decisive role on the photocatalytic performance of FSP-ZnO nanoparticles than the surface area for the ZnO particle size range 8.8–47.0 nm. Fig. 9a shows the corresponding rate constants (on a fixed mass basis) as a function of ZnO crystallite size. The rate constant increased from 0.33 to 1.36 h^{-1} as the crystallite size increased from 8.8 to 47.0 nm and then slightly dropped when the crystallite size was further increased. On the other hand, when the rate constants are presented on an SSA normalized basis (Fig. 9b), an increase of photocatalytic activity of ZnO nanoparticles increased with increasing ZnO particle size from 8.8 to 67.1 nm and then remained relatively constant. The ZnO-47 nm performs best on a mass basis due to its optimum crystallinity and surface area while the ZnO-67.1 nm performs better on a surface area normalized basis, as the crystal quality within the ZnO particles was higher. For the flame-made materials, the crystalline quality would be expected to improve with increasing of the enthalpy density, flame height, and high-temperature residence time. The effect of the crystal size of ZnO on the photocatalytic activity has been reported by many researchers. They also reported the optimum size for which the photocatalytic activity of ZnO is maximized [19–23]. The optimum sizes of ZnO reported in literatures were varied depending on the preparation and pretreatment methods. The decrease of photocatalytic activity of ZnO when the particle size of ZnO was larger than optimum size was explained by the decrease of surface area.

4. Conclusions

The FSP-synthesized ZnO nanoparticles have shown to be better photocatalysts for the degradation of methylene blue dye under UV irradiation, compared to the Degussa P-25 and the JRC-TiO_2 commercial photocatalysts. The photocatalytic activities of the FSP-ZnO nanoparticles were found to be correlated well with their crystalline quality. For those prepared by one-step FSP method with average particle size 8.8–47.0 nm, improved crystal quality as well as higher photocatalytic activities were obtained by increasing flame enthalpy density, flame height, and high-temperature residence time during the FSP synthesis. However, the larger ZnO particle sizes (52.6–103.5 nm) obtained by anneal-

ing post-treatment of the FSP-ZnO at high temperature, showed a descending trend of the photocatalytic activity due to the significant decrease of surface availability for reactant adsorption and light absorption of the annealed ZnO particles.

Acknowledgements

The financial supports from the Thailand Research Fund (TRF) and the Office of Higher Education Commission are gratefully acknowledged.

References

[1] C. Allegre, M. Maisseu, F. Charbit, P. Moulin, Coagulation–flocculation–decantation of dye house effluents: concentrated effluents, J. Hazard. Mater. B 116 (2004) 57–64.
[2] V. Golob, A. Vinder, M. Simonic, Efficiency of the coagulation/flocculation method for the treatment of dyebath effluents, Dyes Pigments 67 (2005) 93–97.
[3] A. Alinsafi, M. Khemis, M.N. Pons, J.P. Leclerc, A. Yacoubi, A. Benhammou, A. Nejmeddine, Electro-coagulation of reactive textile dyes and textile wastewater, Chem. Eng. Proc. 44 (2005) 461–470.
[4] S. Papic, N. Koprivanac, A. LoncaricBozic, A. Metes, Removal of some reactive dyes from synthetic wastewater by combined Al(III) coagulation/carbon adsorption process, Dyes Pigments 62 (2004) 291–298.
[5] K. Tanaka, K. Padermpole, T. Hisanaga, Photocatalytic degradation of commercial azo dyes, Water Res. 34 (2000) 327–333.
[6] N.S. Allen, M. Edge, J. Verran, J. Stratton, J. Maltby, C. Bygott, Photocatalytic titania based surfaces: environmental benefits, Polym. Degrad. Stab. 9 (2008) 1632–1646.
[7] S. Sakthivel, B. Neppolian, M.V. Shankar, B. Arabindoo, M. Palanichamy, V. Murugesan, Solar photocatalytic degradation of azo dye: comparison of photocatalytic efficiency of ZnO and TiO_2, Sol. Energy Mater. Sol. Cells 77 (2003) 65–82.
[8] M.A. Behnajady, N. Modirshahla, R. Hamzavi, Kinetic study on photocatalytic degradation of C.I. Acid Yellow 23 by ZnO photocatalyst, J. Hazard. Mater. 133 (2006) 226–232.
[9] A. Sharma, P. Rao, R.P. Mathur, S.C. Ameta, Photocatalytic reactions of xylidine ponceau on semiconducting zinc oxide powder, J. Photochem. Photobiol. A: Chem. 86 (1995) 197–200.
[10] A.A. Khodja, T. Sehili, J.F. Pilichowski, P. Boule, Photocatalytic degradation of 2-phenylphenol on TiO_2 and ZnO in aqueous suspensions, J. Photochem. Photobiol. A: Chem. 141 (2001) 231–239.
[11] A. Akyol, H.C. Yatmaz, M. Bayramoglu, Photocatalytic decolorization of Remazol Red RR in aqueous ZnO suspensions, Appl. Catal. B: Environ. 54 (2004) 19–24.
[12] R. Kavitha, S. Meghani, V. Jayaram, Synthesis of titania films by combustion flame spray pyrolysis technique and its characterization for photocatalysis, Mater. Sci. Eng. B 139 (2007) 134–140.
[13] N. Daneshvar, D. Salari, A.R. Khataee, Photocatalytic degradation of azo dye acid red 14 in water on ZnO as an alternative catalyst to TiO_2, J. Photochem. Photobiol. A: Chem. 162 (2004) 317–322.
[14] P. Pawinrat, O. Mekasuwandumrong, J. Panpranot, Synthesis of Au–ZnO and Pt–ZnO nanocomposites by one-step flame spray pyrolysis and its application for photocatalytic degradation of dyes, Catal. Commun. 10 (2009) 1380–1385.
[15] A.P. Alivisatos, Perspectives on the physical chemistry of semiconductor nanocrystals, J. Phys. Chem. 100 (1996) 13226–13239.
[16] A. Henglein, Small-particle research: physicochemical properties of extremely small colloidal metal and semiconductor particles, Chem. Rev. 89 (1989) 1861–1873.
[17] M.R. Hoffmann, S.T. Martin, W. Choi, D.W. Bahnemann, Environmental applications of semiconductor photocatalysis, Chem. Rev. 95 (1995) 69–96.
[18] D. Beydoun, R. Amal, G. Low, S. McEvoy, Role of nanoparticles in photocatalysis, J. Nanopart. Res. 1 (1999) 439.
[19] H. Wang, C. Xie, W. Zhang, S. Cai, Z. Yang, Y. Gui, Comparison of dye degradation efficiency using ZnO powders with various size scales, J. Hazard. Mater. 141 (2007) 645–652.
[20] L. Jing, F. Yuan, H. Hou, B. Xin, W. Cai, H. Fu, Relationships of surface oxygen vacancies with photoluminescence and photocatalytic performance of ZnO nanoparticles, Sci. China Ser. B Chem. 48 (2005) 25.
[21] A.C. Dodd, A.J. McKinley, M. Saunders, T. Tsuzuki, Effect of particle size on the photocatalytic activity of nanoparticulate zinc oxide, J. Nanopart. Res. 8 (2006) 43–51.
[22] D. Li, V. Balek, N. Ohashi, T. Mitsuhashi, S. Hishita, H. Haneda, Self-assembly prismatic aggregates formed during the calcination of ZnO powders: in situ monitoring by ETA technique and their photocatalytic properties, J. Colloid Interface Sci. 289 (2005) 472–478.
[23] S.E. Pratsinis, Flame aerosol synthesis of ceramic powders, Prog. Energy Combust. Sci. 24 (1998) 197–219.
[24] T. Tani, L. Ma¨dler, S.E. Pratsinis, Homogeneous ZnO nanoparticles by flame spray pyrolysis, J. Nanopart. Res. 4 (2002) 337–343.
[25] A. Teleki, S.E. Pratsinis, K. Kalyanasundaram, P.I. Goumab, Sensing of organic vapors by flame-made TiO_2 nanoparticles, Sens. Actuators B 119 (2006) 683–690.
[26] H. Briesen, A. Fuhrmann, S.E. Pratsinis, The effect of precursor in flame synthesis of SiO_2, Chem. Eng. Sci. 53 (1998) 4105–4112.
[27] L. Mädler, W.J. Stark, S.E. Pratsinis, Flame-made ceria nanoparticles, J. Mater. Res. 17 (2002) 1356–1362.
[28] S. Hannemann, J. Grunwaldt, P. Lienemann, D. Günther, F. Krumeich, S.E. Pratsinis, A. Baiker, Combination of flame synthesis and high-throughput experimentation: The preparation of alumina-supported noble metal particles and their application in the partial oxidation of methane, Appl. Catal. A: Gen. 316 (2007) 226–239.
[29] M.J. Height, S.E. Pratsinis, O. Mekasuwandumrong, P. Praserthdam, Ag–ZnO catalysts for UV-photodegradation of methylene blue, Appl. Catal. B: Environ. 63 (2006) 305–312.
[30] B. Mariĭ, F.J. Manjoĭn, M. Mollar, J. Cembrero, R. Gómez, Photoluminescence of thermal-annealed nanocolumnar ZnO thin films grown by electrodeposition, Appl. Surf. Sci. 252 (2006) 2826–2831.
[31] J. Lim, K. Shin, H.W. Kim, C. Lee, Effect of annealing on the photoluminescence characteristics of ZnO thin films grown on the sapphire substrate by atomic layer epitaxy, Mater. Sci. Eng. B107 (2004) 301–304.
[32] N. Serpone, D. Lawless, R. Khairlutdinov, E. Pelizzetti, Subnanosecond relaxation dynamics in TiO2 colloidal sols (particle sizes Rp = 1.0–13.4 nm). Relevance to heterogeneous photocatalysis, J. Phys. Chem. 99 (1995) 16655–16661.
[33] A. Umar, S. Lee, Y.H. Im, Y.B. Hahn, Flower-shaped ZnO nanostructures obtained by cyclic feeding chemical vapour deposition: structural and optical properties, Nanotechnology 16 (2005) 2462–2468.
[34] T.S. Vaishnavi, P. Haridoss, C. Vijayan, Optical properties of zinc oxide nanocrystals embedded in mesoporous silica, Mater. Lett. 62 (2008) 1649–1651.
[35] L. Mädler, W.J. Stark, S.E. Pratsinis, Rapid synthesis of stable ZnO quantum dots, J. Appl. Phys. 92 (2002) 6537–6540.
[36] F. Leiter, H. Alves, D. Pfisterer, N.G. Romanov, D.M. Hofmann, B.K. Meyer, Oxygen vacancies in ZnO, Physica B 340–342 (2003) 201–204.
[37] X. Li, B. Zhang, H. Zhu, X. Dong, X. Xia, Y. Cui, K. Huang, G. Du, Properties of ZnO thin films grown on Si substrates by photo-assisted MOCVD, Appl. Surf. Sci. 254 (2008) 2081–2084.
[38] X.Q. Wei, B.Y. Man, M. Liu, C.S. Xue, H.Z. Zhuang, C. Yang, Blue luminescent centers and microstructural evaluation by XPS and Raman in ZnO thin films annealed in vacuum, N-2 and O-2, Physica B 388 (2007) 145–152.
[39] D. Chu, Y. Zeng, D. Jiang, Hydrothermal synthesis and optical properties of Pb^{2+} doped ZnO nanorods, Mater. Lett. 60 (2006) 2783–2785.
[40] K. Vanheusden, W.L. Warren, C.H. Seager, D.R. Tallant, J.A. Voigt, B.E. Gnade, Mechanisms behind green photoluminescence in ZnO phosphor powders, J. Appl. Phys. 79 (1996) 7983–7990.
[41] J. Wang, L. Gao, Hydrothermal synthesis and photoluminescence properties of ZnO nanowires, Solid State Commun. 132 (2004) 269.
[42] Y.V. Kolenko, B.R. Churagulov, M. Kunst, L. Mazerolles, C. Colbeau-Justin, Photocatalytic properties of titania powders prepared by hydrothermal method, Appl. Catal. B: Environ. 54 (2004) 51–58.